Enhancing Memory-Limited Feedforward Neural Networks for State of Charge Estimation through Temporal Feature Engineering

Mostafa Mahdi Yousef
Dept. of Electrical Engineering and Computer Science
York University
Toronto, Canada
mostafa6@yorku.ca

Mohammad Shaterabadi
Dept. of Electrical Engineering and Computer Science
York University
Toronto, Canada
shater94@yorku.ca

Houshang Karimi
Dept. of Electrical Engineering and Computer Science
York University
Toronto, Canada
hkarimi6@yorku.ca

***Abstract*—State-of-charge (SOC) estimation is a key function of Battery Management Systems (BMS) in electric vehicles and battery energy storage systems. However, SOC is not directly measurable, making accurate estimation inherently challenging. Data-driven approaches offer a practical solution by leveraging measurable inputs such as voltage, current, and temperature. Feedforward Neural Networks (FNNs) are attractive due to their low computational complexity, but they lack inherent temporal memory, unlike recurrent architectures. This paper investigates three established casual smoothing techniques—moving average, Butterworth filtering, and exponential moving average—as temporal memory proxies for enhancing FNN-based SOC estimation. Their effectiveness is supported by frequency-domain analysis using the Fast Fourier Transform (FFT), which reveals that key signal dynamics occur at ultra-low frequencies (less than 0.1 mHz), justifying the use of smoothing as memory-preserving transformations. The main contribution of this work is a unified, frequency-informed evaluation framework that systematically benchmarks these techniques under consistent conditions and across varying temperatures. All models are trained and evaluated on LG 18650HG2 Lithium-ion battery data, with 20 repeated runs per model to ensure statistical robustness.**

***Index Terms*—Lithium-ion Batteries, State of Charge Estimation, Feedforward Neural Network, Feature Engineering, Polarization State, Butterworth Filter**

I. Introduction

The electrification of transportation is driving rapid advancements in lithium-ion battery (LIB) technologies, which are widely used in Electric Vehicles (EVs) and energy storage systems due to their superior power and energy density characteristics [1]. Batteries are one of the most expensive parts of an xEV, and Battery Management System (BMS) plays a crucial role in battery safety and longevity [2]. BMS monitors internal battery states, diagnoses faults, and communicates with other components such as on-board/off-board chargers [3]. State of Charge (SOC) is a key parameter for BMS and provides valuable information for other BMS functions and calculations, such as State-of-Health (SOH) estimation and cell balancing.

However, SOC is not a measurable physical quantity and can only be estimated from correlated available signals such as voltage, current, and temperature. Traditional techniques like the Coulomb Counting Method (CCM) and Open Circuit Voltage (OCV) method are computationally light but suffer from error accumulation and long response times, respectively [4]. Model-based approaches using electrical equivalent circuit models have been developed to address the limitations of conventional estimation techniques. Recursive closed-loop filters like Kalman Filter (KF) variants are commonly used for model-based SOC estimation. For instance, in [5], the Extended Kalman Filter (EKF) and Unscented Kalman Filter (UKF), which are known as non-linear KFs, are implemented for SOC estimation, reporting the superior performance of UKF over EKF. In practice, the performance of KF-based methods relies on initial guesses, as well as on process and measurement noise covariances [6]. They also require precise parameter identification and may degrade under variable operating conditions. On the other hand, defining a model that can capture the non-linear behavior of LIBs and account for influential factors such as capacity fading, hysteresis characteristics, and temperature remains challenging. These factors affect parameter values and degrade model accuracy, leading to less accurate estimations, as the performance of model-based approaches is highly dependent on model accuracy [4], [6], [7].

The availability of battery data and recent improvements in machine learning have made data-driven SOC estimation methods a feasible alternative to model-based approaches. Data-driven methods can capture the non-linear behaviors of LIBs without the need to define highly accurate physical models in different operating conditions [8]–[10].

At lower temperatures, the internal resistance of batteries increases and causes higher self-heating (heat generated by RI^2 losses), which creates a noticeable difference between the core and surface temperature of the battery. This temperature gradient between the core and surface brings about lower estimation accuracy as we commonly measure the surface temperature due to cost and technical limitations. However, the core temperature truly reflects the internal chemical reactions and states. On the other hand, lower temperatures increase diffusion delays, and ions cannot move fast enough through the electrolyte and within the electrode materials. During discharging, ions move from anode to cathode. In lower temperatures, they cannot diffuse fast enough to replace the lithium ions removed from the cathode reaction sites (cathode surface), causing a voltage drop more than expected. SOC might be underestimated as a result of this phenomenon. Plenty of lithium ions may still remain deep inside the anode, but they cannot move fast enough to reach the cathode reaction site. During charging in lower temperatures, ions move from the cathode to the anode, and delayed diffusion causes ion accumulation on the anode surface. Reaching deep inside the anode takes longer for injected ions, leading to increase in the measured voltage, and SOC might be overestimated. The underlying challenge in lower temperatures stems from the fact that we are measuring surface signals like surface temperature and voltage. However, they do not reflect the battery's internal state as accurately as higher temperatures, where internal states correlate more closely with surface-level measurements. Thus, as mentioned in [11] and [12], SOC estimation at low temperatures remains a difficult task. Therefore, the chosen estimation method should demonstrate reliable accuracy even under such adverse conditions. A study in [11] demonstrated the acceptable performance of Feedforward Neural Networks (FNNs) across a wide temperature range from $-25°$C to $25°$C, proving their efficacy in lower temperatures. Temporal information was provided to the FNN using a moving average approach, with a final window size of 400 selected from a range of 50-400 time steps. Chapter 7 of [13] compares a Long Short-Term Memory (LSTM) network, as a representative RNN (Recurrent Neural Network), with a memory-aware FNN and concludes that FNN offers comparable—or in some cases- superior performance while requiring significantly lower training time and computational resources.

FNNs have emerged as a popular alternative because of their low computational complexity and ease of training [14], [15], and this makes FNNs a cost-effective and practical solution for embedded system implementation. However, FNNs lack intrinsic memory, which is critical for capturing the inherent temporal dynamics in battery behavior. Previous studies have augmented FNNs with additional input features to embed temporal information [11], [15]–[18]. Based on [13], using more complex architectures with more demanding computational powers does not necessarily guarantee superior performance, and feeding exogenous synthetic inputs into FNN could be an effective way to obtain a competitive performance compared to more complex architectures. Thus, in this study, we select FNN due to its lower computational cost and explore the effective techniques to make FNN a memory-aware architecture like RNNs. Although previous studies have explored various techniques and architectures for SOC estimation, a systematic comparison of temporal feature engineering methods within an FNN context is still lacking. This paper rationalizes using smoothing filters by performing spectral analysis and addresses the gap by evaluating three such techniques on the same dataset, repeated over 20 training iterations, to enable a fair and consistent performance assessment and provide a solid decision framework for future studies.

The remainder of this paper is as follows. Section II describes the basic architecture of the FNN. Section III details the three feature engineering techniques for incorporating temporal dynamics into the FNN. Section IV outlines the experimental setup and dataset pre-processing. Section V presents and discusses the performance evaluation of the proposed methods. Finally, Section VI concludes the paper and suggests future research directions.

II. Feedforward Neural Network Architecture

A feedforward neural network is a type of neural network in which data flows in only one direction—from input to output—during training and inference. This process is known as forward propagation. Equation (1) describes the forward propagation in an FNN for SOC estimation [1]. Here, SOCi is the output of neuron i in the output layer, computed by applying an activation function $f_i(\cdot)$ to the weighted sum of outputs O_j from the previous layer, using weights Wj,k and biases $\theta_{j,k}$. This computation enables the network to learn nonlinear mappings between input features and SOC.

In an FNN, each neuron is typically connected to all neurons in the adjacent layers, forming fully connected (dense) layers. Input data passes through nonlinear activation functions, allowing the network to model complex input-output relationships. The activation functions used in this study, defined in Equations (2), (3), and (4), were selected based on [16].

During each training epoch, the weights and biases are updated using backpropagation to compute gradients, followed by an optimization step based on gradient descent. The batch size determines the number of weight updates and backpropagation steps per epoch. These updates aim to minimize the loss function defined in Equation (5), where $S\hat{O}C(k)$ is the estimated SOC and $SOC(k)$ is the ground truth value.

$$\text{SOC}_i = f_i\left(\sum_k W_{j,k}O_j + \theta_{j,k}\right) \tag{1}$$

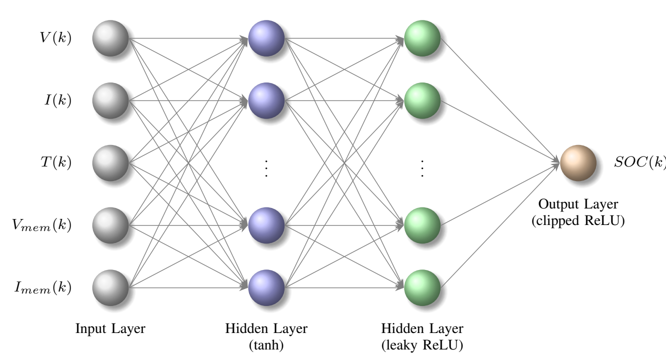

Fig. 1: Feedforward neural network for SOC estimation.

$$y = \tanh(x) = \frac{e^x - e^{-x}}{e^x + e^{-x}} \tag{2}$$

$$y = \text{LeakyReLU}(x) = \begin{cases} x, & x \geq 0 \\ \alpha x, & x < 0 \end{cases} \quad (3)$$

$$y = \text{ClippedReLU}(x) = \begin{cases} 0, & x < 0 \\ x, & 0 \leq x \leq 1 \\ 1, & x > 1 \end{cases} \quad (4)$$

$$J = \frac{1}{K} \sum_k \left(SOC(k) - \hat{SOC}(k) \right)^2 \quad (5)$$

III. Incorporating Temporal Dynamics into FNN

Unlike recurrent neural networks, feedforward neural networks lack memory cells, making them inappropriate for problems dealing with time series. However, we can use feature engineering techniques to create memory-aware FNNs and increase their inference accuracy. To rationalize using smoothing filters to capture required temporal dependencies, we performed a spectral analysis on voltage and current. Based on the Nyquist theorem, we can investigate the spectral content of these signals up to 0.5 HZ (half of the sampling rate). Figure 2 shows the spectral content of the signals and proves the existence of dominant ultra-low frequency components. The energy concentration in both signals is below 0.1 mHz, while the current has higher energy of around 1 mHz. This frequency-domain investigation confirms that voltage and current are band-limited signals, and smoothing filters can capture and feed important information to FNN architecture. Figure 2 provides crucial information for tuning the window sizes and cutoff frequencies of designed filters to generate synthetic inputs fed to training networks. In this study, we investigate three distinct methods to infuse temporal dynamics into FNN-based SOC estimation:

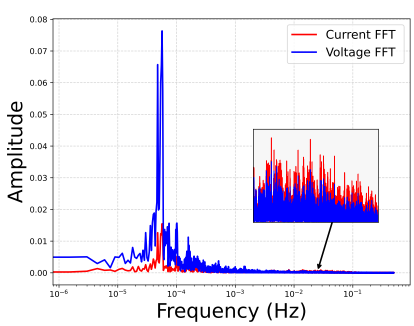

Fig. 2: Frequency Spectra of Current and Voltage Signals

- **MA-FNN:** Utilizing moving average filtering to smooth instantaneous voltage and current measurements, thereby summarizing recent signal history.
- **BW-FNN:** Applying Butterworth low-pass filtering to extract both short- and long-term trends from the raw data.
- **PS-FNN:** This approach incorporates a recursively defined Polarization State (PS), serving as an effective proxy for memory while avoiding the complexity of recurrent architectures. Specifically, PS is implemented as an Exponential Moving Average (EMA). To align with the terminology used in [17], where EMA was applied in a hybrid architecture to smooth current signals, we refer to it as PS in this study.

By directly comparing these three methods on LG 18650HG2 battery data [16] collected under challenging conditions (e.g., low temperature), we aim to fill a notable research gap highlighted in section I.

A. Moving Average-Based Temporal Feature

By using the moving average and selecting a suitable window size based on the signal characteristics, we can feed memory-like information of the main inputs in the SOC estimation problem into FNN. $U_{avg}(k) \in \{V_k, I_k\}$ refers to the moving average of measured voltages and currents used to train and test the model. As shown in Equation 6, the moving average of voltage and current captures recent signal history. In this equation, n is the window size, and k is the current time step.

$$U_{\text{avg}}(k) = \begin{cases} \frac{1}{k} \sum_{j=1}^{k} U(j), & \text{if } k < n \\ \frac{1}{n} \sum_{j=k-n+1}^{k} U(j), & \text{if } k \geq n \end{cases} \quad (6)$$

B. Butterworth Filter-Based Temporal Feature

By Butterworth filtering technique, we can extract short-term and long-term evolution of input voltage and current and provide temporal features to FNN. In Equation 7, $U(k)$ represents the raw input at discrete time step k, and $U_{\text{filt}}(k)$ is the corresponding filtered output. The coefficients $\{b_i\}$ and $\{a_j\}$ are determined by the Butterworth filter design, where M and N denote the filter order. The first summation represents the feedforward (input) path, and the second summation represents the feedback (output) path of the digital Infinite Impulse Response filter.

$$U_{\text{filt}}(k) = \sum_{i=0}^{M} b_i U(k-i) - \sum_{j=1}^{N} a_j U_{\text{filt}}(k-j) \quad (7)$$

C. Recursive Polarization State-Based Temporal Feature

To compensate for the lack of memory in FNNs, we can incorporate an auxiliary input termed the *polarization state*, which is a recursively filtered version of the current. This signal provides temporal context without increasing network complexity.

The polarization state at sampling step k is defined as:

$$EMA_k = e^{-\frac{\Delta t}{\tau}} EMA_{k-1} + \left(1 - e^{-\frac{\Delta t}{\tau}}\right) U_k \quad (8)$$

where Δt is the sampling interval, τ is a time constant. This formulation captures recent current history and acts as a temporal feature for SOC estimation.

Although named "polarization state", this signal should not be confused with electrochemical polarization voltage. It is a synthetic memory proxy, defined purely based on exponential moving average.

To reduce redundancy from using multiple τ values, highly correlated polarization states are removed using:

$$r(x,y) = \frac{\mathrm{Cov}(x,y)}{\sqrt{\mathrm{Var}[x] \cdot \mathrm{Var}[y]}} \tag{9}$$

When $r(x,y)$ exceeds a threshold (e.g., 0.95), one of the signals is discarded. The remaining polarization states are concatenated with other input features and provided to the FNN.

IV. Training Dataset

This study uses a publicly available dataset related to a brand-new LG 18650HG2 battery cell with 3 Ah capacity and 3.6 V nominal voltage [16]. Isothermal tests were conducted from $-10\,^\circ$C to $25\,^\circ$C, during which voltage, current, temperature, and consumed/supplied Ampere-Hour were recorded. As mentioned in Section I, SOC estimation becomes more difficult at lower temperatures, and the $-10\,^\circ$C dataset is particularly useful for evaluating the robustness of the proposed techniques under such conditions. SOC ground truth is calculated using Equation 10.

Since measurements were taken at varying sample rates, all data were resampled to 1 Hz for consistency, and outliers were removed. Realistic drive cycles—including UDDS, HWFET, LA92, US06, and eight synthetic Mixed 1–8 cycles—were used for discharging until about 95% depletion. These cycles simulate a range of driving behaviors: UDDS reflects mild urban driving, HWFET models highway cruising, US06 captures aggressive driving with rapid load changes, and LA92 represents mixed suburban-urban patterns. Mixed 1–8 further introduce variability by combining random segments of standard cycles. For charging, a 1-C rate CC-CV strategy was applied: 1.5 A constant current until 4.2 V, followed by constant voltage until the current had dropped to 50 mA. To account for sensor noise, the dataset includes 13 noisy variants of V, I, and T based on gain and offset errors defined in [16], along with the original signals—all labeled with the same SOC. This enhances the model's robustness during real-world inference. Finally, all features are normalized using min–max normalization (Equation 11) to scale them between 0 and 1. The full dataset is split into training, validation, and four test sets, as detailed in Table I, with each set containing three discharge segments representing UDDS, LA92, and US06.

$$SOC = \frac{\text{Supplied/ Consumed AH}}{\text{Nominal AH}} \tag{10}$$

$$x_{\text{normalized}} = \frac{x - \min(x)}{\max(x) - \min(x)} \tag{11}$$

TABLE I: Dataset Size and Partitions

Dataset Partition	Data Points
Training (75%)	669,958
Validation (5%)	39,295
Testing ($-10\,^\circ$C)	39,293
Testing ($0\,^\circ$C)	42,530
Testing ($10\,^\circ$C)	44,284
Testing ($25\,^\circ$C)	47,517
Total	**882,877**

TABLE II: Hyperparameter Configuration for Feedforward Neural Network

Hyperparameter	Configuration
Number of Hidden Layers	2 (55 Neurons per Hidden Layer)
Hidden Layer Activations	Tanh, Leaky ReLU ($\alpha = 0.3$)
Output Activation	Clipped ReLU (max = 1.0)
Loss Function	Mean Squared Error (MSE)
Optimization Method	Adam
Initial Learning Rate	0.01
Training Epochs	5500
Batch Size	Full-batch (entire training set)
Shuffle Policy	Disabled (no shuffling)
Validation Strategy	Fixed (-10 °C test set)

V. Experimental Results and Performance Evaluation

To validate the smoothing methods, we conducted experiments using the multi-temperature LG 18650HG2 dataset (Section IV). Each model was trained 20 times to reduce the impact of random initialization. Average RMSE and MAE were computed using Equations 12 and 13, with hyperparameters from [13] listed in Table II. The window size of the moving average is 500, and Butterworth cutoff frequencies are 0.5 mHz and 5 mHZ, representing long-term and short-term dependencies, respectively. Based on the defined equations in Section III, time constants for the PS method are selected. For each signal, a weighted sum of its associated polarization states is computed and used as input to the FNN. The smoothing filter parameters are selected by evaluating the trained model's performance across various configurations within a range determined by FFT analysis.

$$\mathrm{RMSE}_{\text{avg}} = \frac{1}{N}\sum_{n=1}^{N}\sqrt{\frac{1}{K}\sum_{k=1}^{K}\left(\mathrm{SOC}_k - \hat{\mathrm{SOC}}_k^{(n)}\right)^2} \tag{12}$$

$$\mathrm{MAE}_{\text{avg}} = \frac{1}{N}\sum_{n=1}^{N}\frac{1}{K}\sum_{k=1}^{K}\left|\mathrm{SOC}_k - \hat{\mathrm{SOC}}_k^{(n)}\right| \tag{13}$$

TABLE III: Performance of Baseline FNN Without Temporal Smoothing

Metric	-10 °C	0 °C	10 °C	25 °C	Avg
RMSE	4.23%	3.36%	3.26%	2.61%	3.36%
MAE	2.75%	2.22%	2.38%	1.58%	2.23%

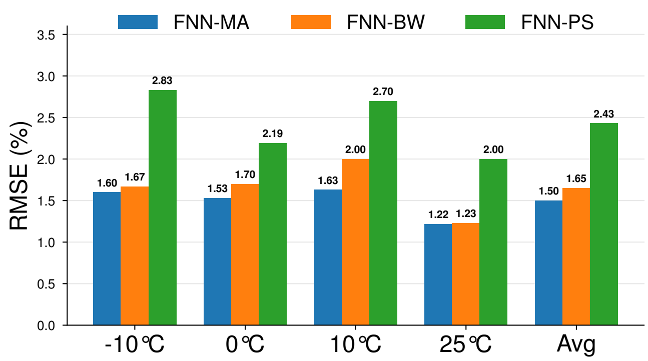

Fig. 3: RMSE comparison of FNN variants with temporal smoothing across test temperatures.

FNN performance without the discussed filters is presented in Table III as a baseline for comparison. After encoding temporal information into the FNN, the $RMSE_{avg}$ and MAE_{avg} values are reported in Figures 3 and 4, respectively. Based on experimental results, all filtering techniques significantly improved inference accuracy compared to the baseline FNN. Among them, Butterworth demonstrated superior performance across all temperatures, achieving an MAE of 0.96%, which is very close to that of MA but with a slightly higher RMSE. This higher RMSE in Butterworth occurs particularly during transitions between charging and discharging states. However, as Figures 5 to 7 illustrate, Butterworth generally outperforms other filters. Figure 8 shows a higher error during discharges compared to charging cycles across all investigated driving conditions. This fact motivates exploring hybrid techniques to decrease prediction error in these segments. On the other hand, PS consistently showed the poorest performance across all temperatures, exhibiting high-frequency noise during inference in all drive cycles. This demonstrates its ineffectiveness and inability to capture long-term trends necessary for accurate SOC estimation.

Future research will focus on fusing model-based and data-driven algorithms to diminish the higher error noted during discharge cycles and further increase estimator robustness in challenging conditions such as transient load changes due to aggressive driving conditions and lower temperatures. To further validate the effectiveness of these methods on real-time applications, a Hardware-in-the-Loop (HIL) test will be conducted on other battery chemistries to examine the generalization of hybrid approaches.

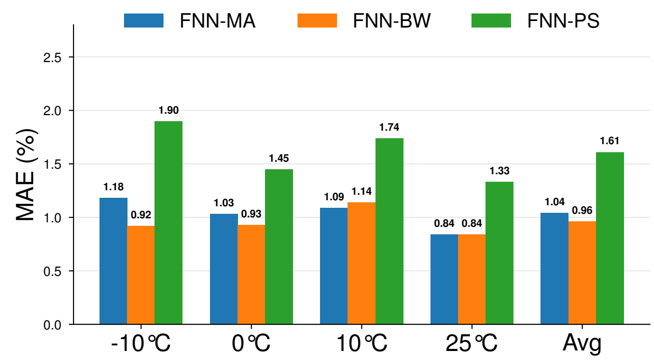

Fig. 4: MAE comparison of FNN variants with temporal smoothing across test temperatures.

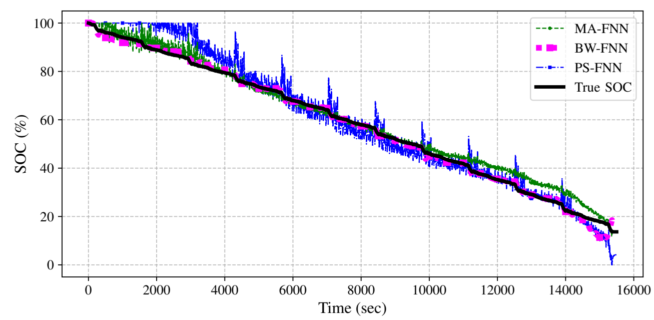

Fig. 5: SOC estimation results on the UDDS at 25 °C using FNN variants.

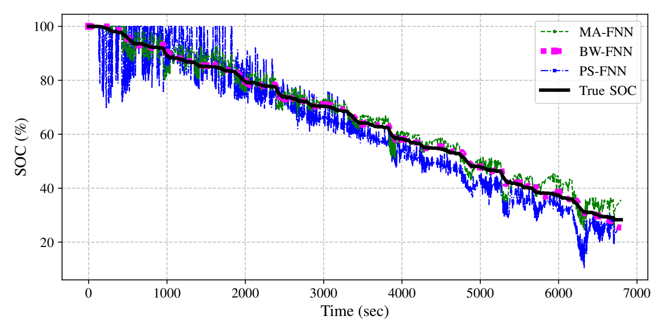

Fig. 6: SOC estimation results on the LA92 at $-10\,°C$ using FNN variants.

VI. Conclusion

This paper has systematically analyzed temporal feature engineering techniques to enhance memory-limited feedforward neural networks for lithium-ion battery state-of-charge estimation. Frequency-domain analysis revealed the energy concentration of the spectral content in lower frequencies (less than 0.1 mHz), validating the effectiveness of casual smoothing techniques in capturing important temporal features. Cutoff frequencies, time constants, and window size of the smoothing filters were tuned based on FFT results and performance evaluation within a specified range. All

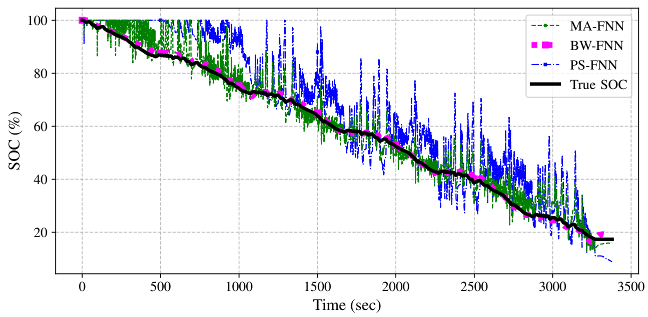

Fig. 7: SOC estimation results on the US06 at 10 °C using FNN variants.

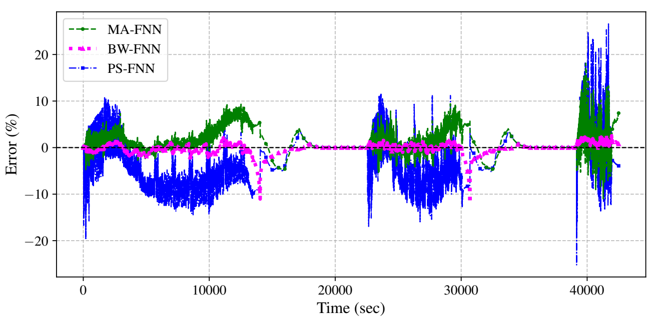

Fig. 8: SOC estimation error over all drive cycles at 0 °C for different FNN variants.

the techniques outperformed baseline FNN, and Butterworth showed superior MAE despite slightly higher RMSE than MA. The exponential moving average had the worst performance, which can be rationalized with FTT analysis as EMA weighs recent data more than past information. Future work involves proposing hybrid approaches to improve the robustness of BW-FNN while keeping the mean average error lower than the simple moving average.

References

[1] D. N. T. How, M. A. Hannan, M. S. H. Lipu, and P. J. Ker, "State of charge estimation for lithium-ion batteries using model-based and data-driven methods: A review," *IEEE Access*, vol. 7, pp. 136 116–136 136, 2019.

[2] A. M. Andwari, A. Pesiridis, S. Rajoo, R. Martinez-Botas, and V. Esfahanian, "A review of battery electric vehicle technology and readiness levels," *Renewable and Sustainable Energy Reviews*, vol. 78, pp. 414–430, 2017.

[3] B. Bilgin, P. Magne, P. Malysz, Y. Yang, V. Pantelic, M. Preindl, A. Korobkine, W. Jiang, M. Lawford, and A. Emadi, "Making the case for electrified transportation," *IEEE Transactions on Transportation Electrification*, vol. 1, no. 1, pp. 4–17, 2015.

[4] Y. Wang, J. Tian, Z. Sun, L. Wang, R. Xu, M. Li, and Z. Chen, "A comprehensive review of battery modeling and state estimation approaches for advanced battery management systems," *Renewable and Sustainable Energy Reviews*, vol. 131, p. 110015, 2020.

[5] R. P. Priya and R. Sakile, "State of charge estimation of lithium-ion battery based on extended kalman filter and unscented kalman filter techniques," *Energy Storage*, vol. 5, no. 3, p. e408, 2023.

[6] P. Shrivastava, T. K. Soon, M. Y. I. B. Idris, and S. Mekhilef, "Overview of model-based online state-of-charge estimation using kalman filter family for lithium-ion batteries," *Renewable and Sustainable Energy Reviews*, vol. 113, p. 109233, 2019.

[7] M. A. Hannan, M. S. H. Lipu, A. Hussain, and A. Mohamed, "A review of lithium-ion battery state of charge estimation and management system in electric vehicle applications: Challenges and recommendations," *Renewable and Sustainable Energy Reviews*, vol. 78, pp. 834–854, 2017.

[8] M. Ragone, V. Yurkiv, A. Ramasubramanian, B. Kashir, and F. Mashayek, "Data driven estimation of electric vehicle battery state-of-charge informed by automotive simulations and multi-physics modeling," *Journal of Power Sources*, vol. 483, p. 229108, 2021.

[9] Z. Cui, L. Wang, Q. Li, and K. Wang, "A comprehensive review on the state of charge estimation for lithium-ion battery based on neural network," *Energy Storage Materials*, vol. 3, no. 2, pp. 123–139, 2021.

[10] B. D. Soyoye, I. Bhattacharya, M. V. A. Dhason, and T. Banik, "State of charge and state of health estimation in electric vehicles: Challenges, approaches and future directions," *Batteries*, vol. 11, no. 1, p. 32, 2025.

[11] E. Chemali, P. J. Kollmeyer, M. Preindl, and A. Emadi, "State-of-charge estimation of li-ion batteries using deep neural networks: A machine learning approach," *Journal of Power Sources*, vol. 400, pp. 242–255, 2018.

[12] J. Wu, T. Li, H. Zhang, Y. Lei, and G. Zhou, "Research on modeling and soc estimation of lithium iron phosphate battery at low temperature," *Energy Procedia*, vol. 152, pp. 556–561, 2018.

[13] C. J. G. Vidal, "State-of-charge estimation of lithium-ion batteries for electrified powertrains using neural networks," Ph.D. dissertation, McMaster University, Hamilton, Ontario, Canada, 2020. [Online]. Available: http://hdl.handle.net/11375/25851

[14] J. Tian, C. Chen, W. Shen, F. Sun, and R. Xiong, "Deep learning framework for lithium-ion battery state of charge estimation: Recent advances and future perspectives," *Energy Storage Materials*, vol. 61, p. 102883, 2023.

[15] D. Zhang, C. Zhong, P. Xu, and Y. Tian, "Deep learning in the state of charge estimation for li-ion batteries of electric vehicles: A review," *Machines*, vol. 10, p. 912, Oct 2022.

[16] P. Kollmeyer, C. Vidal, M. Naguib, and M. Skells, "Lg 18650hg2 li-ion battery data and example deep neural network xev soc estimator script," Mendeley Data, V3, 2020, available: https://doi.org/10.17632/cp3473x7xv.3.

[17] C. Chen, R. Xiong, R. Yang, W. Shen, and F. Sun, "State-of-charge estimation of lithium-ion battery using an improved neural network model and extended kalman filter," *Journal of Cleaner Production*, vol. 234, pp. 1153–1164, 2019.

[18] T. Hao, J. Ding, and T. Tu, "A hybrid kalman filter for soc estimation of lithium-ion batteries," in *2022 41st Chinese Control Conference (CCC)*. IEEE, 2022, pp. 5222–5227.